An Embedded Discontinuous Galerkin Method for the Compressible Euler and Navier-Stokes Equations

J. Peraire[*] and N. C. Nguyen[†]

Massachusetts Institute of Technology, Cambridge, MA 02139, USA

B. Cockburn[‡]

University of Minnesota, Minneapolis, MN 55455, USA

We present an Embedded Discontinuous Galerkin (EDG) method for the solution of the compressible Euler and Navier-Stokes equations. The method is devised by using the discontinuous Galerkin approximation with a special choice of the numerical fluxes and weakly imposing the continuity of the normal component of the numerical fluxes across the element interfaces. This allows the approximate conserved variables defining the discontinuous Galerkin solution to be locally condensed, thereby resulting in a reduced system which involves only the degrees of freedom of the approximate traces of the solution. The EDG method can be seen as a particular form of a Hybridizable Discontinuous Galerkin (HDG) method in which the hybrid fluxes are required to belong to a smaller space than in standard HDG methods. In our EDG method, the hybrid unknown is taken to be continuous at the vertices, thus resulting in an even smaller number of coupled degrees of freedom than in the HDG method. In fact, the resulting stiffness matrix has the same structure as that of the statically condensed continuous Galerkin method. In exchange for the reduced number of degrees of freedom, the EDG method looses the optimal converge property of the flux which characterizes other HDG methods. Thus, for convection-diffusion problems, the EDG solution converges optimally for the primal unknown but suboptimally for the flux.

I.   Introduction

Discontinuous Galerkin (DG) finite element methods have emerged as a competitive alternative over classical finite differences and finite volume methods for solving nonlinear hyperbolic systems of conservation laws. DG methods work well on unstructured meshes and result in stable high order discretizations of the convective and diffusive operators. Despite all these advantages, DG methods have not yet made a significant impact for practical applications. This is largely due to the high computational cost associated with DG methods for large scale practical applications.

In [21], we presented an extension of the Hybridized Discontinuous Galerkin (HDG) method [6–8, 12–18] to the numerical solution of the compressible Euler and Navier-Stokes equations. HDG methods possess local conservativity, high-order accuracy, and strong stability for convection-dominated flows and result in a final system involving only the degrees of freedom of the approximate traces of the field variables. Since the approximate traces are defined on the element faces only and are single-valued on every face, the HDG methods have significantly less the globally coupled unknowns than other DG methods. In addition, the HDG method is the only DG method that exhibits optimal convergence properties for the primal variables as well as their fluxes.

We present an Embedded Discontinuous Galerkin (EDG) method for the solution of the compressible Euler and Navier-Stokes equations. The EDG method considered here is a particular form of HDG method in which the hybrid fluxes are required to belong to a smaller space than in standard HDG methods. In

---

[*]Professor, Department of Aeronautics and Astronautics, M.I.T., 77 Massachusetts Avenue, AIAA Associate Fellow.
[†]Research Scientist, Department of Aeronautics and Astronautics, M.I.T., 77 Massachusetts Avenue, AIAA Member.
[‡]Professor, School of Mathematics, University of Minnesota, Minneapolis.

our EDG method, the hybrid unknown is taken to be continuous at the vertices, thus resulting in an even smaller number of coupled degrees of freedom than in the HDG method. In fact, the resulting stiffness matrix has the same structure as that of the statically condensed continuous Galerkin method. The EDG method was first introduced in[10] for the solution of shell problems. It was later presented for symmetric elliptic problems in[6] and analyzed in.[9] It turns out that in exchange for the reduced number of degrees of freedom, the EDG method looses the optimal converge property of the flux which characterizes other HDG methods. Thus, the for convection-diffusion problem, the EDG solution converges optimally for the primal unknown but suboptimally for the flux. In that respect, the EDG method is comparable to all other existing DG schemes (except HDG) but has much fewer globally coupled degrees of freedom than both standard DG and HDG methods.

The HDG and EDG methods are devised by using the discontinuous Galerkin methodology to discretize the compressible Navier-Stokes equations with appropriate choices of the numerical fluxes and by applying the hybridization technique to the resulting discretization. We first introduce the approximate traces of the conserved variables as new unknowns defined on the element boundaries. The only difference between standard HDG methods and the EDG method considered here is the space in which the approximated traces of the solution are defined. The space of the HDG method contains functions which are defined on the element faces and are allowed to be discontinuous at the element vertices (and edges in 3D) where the different faces intersect. On the other hand, the trace space of the EDG method is restricted to functions in the original HDG trace space which are continuous at the element vertices (and edges in 3D). The total numerical flux (including both the viscous and inviscid terms) is defined in terms of the approximate traces and continuity of the normal component of the numerical flux is imposed weakly. This results in a large nonlinear system of equations for the approximate field variables (including velocity, density, and energy and their spatial derivatives) an the trace of the conserved variables. This nonlinear system is solved by using the Newton method. After linearization, we can locally condense all the approximate field variables and their spatial derivatives in an element-by-element fashion and obtain a reduced global system involving only the approximate traces of the conserved variables.

Below, we describe the HDG method for the compressible Euler equations and then introduce the EDG discretization. We then extend these methods to the time dependent problem and the Navier-Stokes equations. Finally, we present extensive numerical experiments to demonstrate and compare their performance.

II.   The Euler Equations

A.   Governing Equations and Notation

We consider the steady-state Euler equations of gas dynamics defined over a domain $\Omega \subset \mathcal{R}^d$ written in nondimensional conservation form as

$$\nabla \cdot \boldsymbol{F}(\boldsymbol{u}) \;=\; 0, \qquad \text{in } \Omega, \tag{1}$$

where $\boldsymbol{u}$ is the m-dimensional vector of conserved dimensionless quantities (namely, density, momentum and energy) and $\boldsymbol{F}(\boldsymbol{u})$ are the inviscid fluxes of dimension $m \times d$. The Euler equations (1) must be supplemented with appropriate boundary conditions at the inflow and outflow boundaries and at the solid wall.

To describe the HDG method for solving the Euler equations, we introduce some notation. We denote by $\mathcal{T}_h$ a collection of disjoint regular elements K that partition Ω and set $\partial \mathcal{T}_h := \{\partial K : K \in \mathcal{T}_h\}$. For an element K of the collection $\mathcal{T}_h$, $F = \partial K \cap \partial \Omega$ is the boundary face if the $d-1$ measure of F is nonzero. For two elements K^+ and K^- of the collection $\mathcal{T}_h$, $F = \partial K^+ \cap \partial K^-$ is the interior face between K^+ and K^- if the $d-1$ measure of F is nonzero. We denote by $\mathcal{E}_h^o$ and $\mathcal{E}_h^\partial$ the set of interior and boundary faces, respectively. We set $\mathcal{E}_h = \mathcal{E}_h^o \cup \mathcal{E}_h^\partial$.

Let $\mathcal{P}^k(D)$ denote the space of polynomials of degree at most k on a domain D and let $L^2(D)$ be the space of square integrable functions on D. We introduce the following discontinuous finite element approximation space

$$\boldsymbol{W}_h^k = \{\boldsymbol{w} \in (L^2(\mathcal{T}_h))^m \; : \; \boldsymbol{w}|_K \in (\mathcal{P}^k(K))^m, \; \forall\, K \in \mathcal{T}_h\}.$$

In addition, we introduce a finite element approximation space for the approximate trace of the solution

$$\boldsymbol{M}_h^k = \{\boldsymbol{\mu} \in (L^2(\mathcal{E}_h))^m \; : \; \boldsymbol{\mu}|_F \in (\mathcal{P}^k(F))^m, \; \forall\, F \in \mathcal{E}_h\}. \tag{2}$$

American Institute of Aeronautics and Astronautics

Note that $\boldsymbol{M}_h^k$ consists of functions which are continuous inside the faces (or edges) $F \in \mathcal{E}_h$ and discontinuous at their borders.

Finally, we define various inner products for our finite element spaces. We write $(w, v)_{\mathcal{T}_h} := \sum_{K \in \mathcal{T}_h}(w, v)_K$, where $(w, v)_D$ denotes the integral of $w\,v$ over the domain $D \subset \mathbb{R}^d$ for $w, v \in P_h$. We also write $(\boldsymbol{w}, \boldsymbol{v})_{\mathcal{T}_h} := \sum_{i=1}^{m}(w_i, v_i)_{\mathcal{T}_h}$ for $\boldsymbol{w}, \boldsymbol{v} \in \boldsymbol{W}_h^k$. We then write $\langle \eta, \zeta \rangle_{\partial \mathcal{T}_h} := \sum_{K \in \mathcal{T}_h} \langle \eta, \zeta \rangle_{\partial K}$ and $\langle \boldsymbol{\eta}, \boldsymbol{\zeta} \rangle_{\partial \mathcal{T}_h} := \sum_{i=1}^{m} \langle \eta_i, \zeta_i \rangle_{\partial \mathcal{T}_h}$, for $\boldsymbol{\eta}, \boldsymbol{\zeta} \in \boldsymbol{M}_h^k$, where $\langle \eta, \zeta \rangle_D$ denotes the integral of $\eta\,\zeta$ over the domain $D \subset \mathbb{R}^{d-1}$.

B.   The HDG Method for the Euler Equations

We seek an approximation $\boldsymbol{u}_h \in \boldsymbol{W}_h^k$ such that for all $K \in \mathcal{T}_h$,

$$- (\boldsymbol{F}(\boldsymbol{u}_h), \nabla \boldsymbol{w})_K + \left\langle \widehat{\boldsymbol{F}}_h \cdot \boldsymbol{n}, \boldsymbol{w} \right\rangle_{\partial K} \;=\; 0, \quad \forall \boldsymbol{w} \in (\mathcal{P}^k(K))^m. \tag{3}$$

Here, the numerical flux $\widehat{\boldsymbol{F}}_h$ is an approximation to $\boldsymbol{F}(\boldsymbol{u})$ over ∂K. We take the numerical flux of the form

$$\widehat{\boldsymbol{F}}_h \cdot \boldsymbol{n} = \boldsymbol{F}(\widehat{\boldsymbol{u}}_h) \cdot \boldsymbol{n} + \boldsymbol{S}(\boldsymbol{u}_h, \widehat{\boldsymbol{u}}_h)(\boldsymbol{u}_h - \widehat{\boldsymbol{u}}_h), \quad \text{on } \partial K, \tag{4}$$

where $\widehat{\boldsymbol{u}}_h \in \boldsymbol{M}_h^k$ is an approximation to the trace of the solution $\boldsymbol{u}$ on ∂K, and $\boldsymbol{S}(\boldsymbol{u}_h, \widehat{\boldsymbol{u}}_h)$ is a local stabilization matrix which has an important effect on both the stability and accuracy of the resulting scheme. Here, the stabilization matrix is inspired by the local Lax-Friedrich method and has the form

$$\boldsymbol{S} = (|\widehat{\boldsymbol{u}}_h \cdot \boldsymbol{n}| + c_h)\boldsymbol{I}, \tag{5}$$

where c_h is the sound speed and $\boldsymbol{I}$ is the identity matrix. Note also that $\widehat{\boldsymbol{u}}_h$ is single-valued over each face since $\widehat{\boldsymbol{u}}_h$ belongs to $\boldsymbol{M}_h^k$. However, $\widehat{\boldsymbol{u}}_h$ is discontinuous at the border between two faces.

By adding the contributions of (3) over all the elements and enforcing the continuity of the normal component of the numerical flux, we arrive at the following problem: find an approximation $(\boldsymbol{u}_h, \widehat{\boldsymbol{u}}_h) \in \boldsymbol{W}_h^k \times \boldsymbol{M}_h^k$ such that

$$\begin{aligned}
- (\boldsymbol{F}(\boldsymbol{u}_h), \nabla \boldsymbol{w})_{\mathcal{T}_h} + \left\langle \widehat{\boldsymbol{F}}_h \cdot \boldsymbol{n}, \boldsymbol{w} \right\rangle_{\partial \mathcal{T}_h} &= 0, & \forall \boldsymbol{w} \in \boldsymbol{W}_h^k, \\
\left\langle \widehat{\boldsymbol{F}}_h \cdot \boldsymbol{n}, \boldsymbol{\mu} \right\rangle_{\partial \mathcal{T}_h \setminus \partial \Omega} + \left\langle \widehat{\boldsymbol{B}}_h, \boldsymbol{\mu} \right\rangle_{\partial \Omega} &= 0, & \forall \boldsymbol{\mu} \in \boldsymbol{M}_h^k.
\end{aligned} \tag{6}$$

Here $\widehat{\boldsymbol{B}}_h$ is the numerical flux vector of dimension m and is defined over the boundary $\partial \Omega$. The precise definition of the boundary numerical flux $\widehat{\boldsymbol{B}}_h$ depends on the types of boundary conditions and can be found in [21].

C.   The EDG Method for the Euler Equations

Compared to the standard discontinuous Galerkin method, the HDG method results in reduced number of globally coupled number of degrees of freedom. In order to further decrease the number of global degrees of freedom, we reduce the space $\boldsymbol{M}_h$ by requiring that its member functions are continuous on $\mathcal{E}_h$. In particular, we define

$$\widetilde{\boldsymbol{M}}_h^k = \boldsymbol{M}_h \cap \mathcal{C}^0(\mathcal{E}_h) \tag{7}$$

where $\boldsymbol{M}_h^k$ is defined in (2).

The EDG method can now be defined as: find an approximation $(\boldsymbol{u}_h, \widehat{\boldsymbol{u}}_h) \in \boldsymbol{W}_h^k \times \widetilde{\boldsymbol{M}}_h^k$ such that

$$\begin{aligned}
- (\boldsymbol{F}(\boldsymbol{u}_h), \nabla \boldsymbol{w})_{\mathcal{T}_h} + \left\langle \widehat{\boldsymbol{F}}_h \cdot \boldsymbol{n}, \boldsymbol{w} \right\rangle_{\partial \mathcal{T}_h} &= 0, & \forall \boldsymbol{w} \in \boldsymbol{W}_h^k, \\
\left\langle \widehat{\boldsymbol{F}}_h \cdot \boldsymbol{n}, \boldsymbol{\mu} \right\rangle_{\partial \mathcal{T}_h \setminus \partial \Omega} + \left\langle \widehat{\boldsymbol{B}}_h, \boldsymbol{\mu} \right\rangle_{\partial \Omega} &= 0, & \forall \boldsymbol{\mu} \in \widetilde{\boldsymbol{M}}_h^k.
\end{aligned} \tag{8}$$

where $\widehat{\boldsymbol{F}}_h \cdot \boldsymbol{n}$ is given by (4) and $\widehat{\boldsymbol{B}}_h$ is the same as in (6). Note that the EDG method (8) is similar to the HDG method (6) except that $\widehat{\boldsymbol{u}}_h$ is not only single-valued over each faces but also continuous at the element vertices (and edges in 3D) since $\widehat{\boldsymbol{u}}_h$ belongs to $\widetilde{\boldsymbol{M}}_h^k$.

American Institute of Aeronautics and Astronautics

By applying the Newton-Raphson procedure to solve the weak formulation (6) we obtain at every Newton step a matrix system of the form

$$\begin{bmatrix} A & B \\ C & D \end{bmatrix} \begin{pmatrix} U \\ \Lambda \end{pmatrix} = \begin{pmatrix} F \\ G \end{pmatrix},$$

where U and Λ are the vectors of degrees of freedom of $\boldsymbol{u}_h$ and $\widehat{\boldsymbol{u}}_h$, respectively. It is important to note that the matrix A has block-diagonal structure. Therefore, we can eliminate U to obtain a reduced system in terms of Λ as

$$\mathbb{K}\Lambda = \mathbb{R},$$

where $\mathbb{K} = D - CA^{-1}B$ and $\mathbb{R} = G - CA^{-1}F$. This is the global system to be solved at every Newton iteration. Since $\widehat{\boldsymbol{u}}_h$ is defined and single-valued along the faces and vertices, the final matrix system of the EDG method is much smaller than that of standard DG methods. In fact, the matrix K has the same structure as the stiffness matrix obtained in continuous Galerkin formulations after static condenstation of the interior nodes has been carried out.

D. Cost comparison between EDG and other methods

In this section, we compare the EDG method to two other classes of DG methods, the HDG method[12, 13] and other DG methods such as the CDG method[22] or the method of Bassi and Reaby.[3] We consider a discretization into simplices in 2D and 3D and polynomial approximations of order $k = 1, \ldots, 5$. We compare the total number of globally coupled degrees of freedom as well as the number of non-zero elements in the jacobian matrix. It turns out that for implicit iterative solvers, the number of non zero elements in the jacobian matrix provides a good indication of the overall computational cost. We consider large meshes so that the boundary effects become unimportant. Also, we assume that in a 3D mesh, the number of tetrahedra is about five times the number of vertices and that the number of tetrahedra sharing a vertex is about twenty. These assumptions are reasonable for well shaped meshes.

We consider a mesh of simplices with N_p vertices. For a system of conservation laws involving N_c components ($N_c = 4$ for laminar the Navier-Stokes equations in $2D$ and $N_c = 5$ in the 3D case), the total number of degrees of freedom is given by

$$DOF = N_p N_c \alpha_{\mathrm{DOF}}, \tag{9}$$

where the coefficient α_{DOF} is given in Table 1. The total number of non-zero entries in the jacobian matrix is given by

$$NNZ = N_p N_c^2 \alpha_{\mathrm{NNZ}}. \tag{10}$$

The coefficient α_{NNZ} is given in Table 2.

2D		k=1	k=2	k=3	k=4	k=5
DG		6	12	20	30	42
HDG		6	9	12	15	18
EDG		**1**	**4**	**7**	**10**	**13**

3D		k=1	k=2	k=3	k=4	k=5
DG		20	50	100	175	280
HDG		30	60	100	150	210
EDG		**1**	**6**	**21**	**46**	**81**

Table 1. Values of the coefficient α_{DOF} as a function of the number of spatial dimensions, the approximating polynomial order and the numerical discretization algorithm. This coefficient can be used in expression (9) to determine the total number of degrees of freedom in the problem.

In all cases, we observe a dramatic reduction in computational cost when the EDG is considered. We also note that the total number of degrees of freedom in HDG and EDG scales like k in 2D and k^2 in 3D. This compares very favorably to a scaling of k^2 and k^3 in 2D and 3D, respectively, for the DG method. If we look at the number of non-zero entries in the matrix, the scaling of the EDG and HDG methods is like k^2 in 2D and k^4 in 3D, wheres for the DG method, the scaling is like k^4 in 2D and k^6 in 3D.

American Institute of Aeronautics and Astronautics

2D

	k=1	k=2	k=3	k=4	k=5
DG	72	288	800	1,800	3,528
HDG	60	135	240	375	540
EDG	**7**	**46**	**115**	**214**	**343**

3D

	k=1	k=2	k=3	k=4	k=5
DG	400	2,500	10,000	30,625	78,400
HDG	630	2,520	7,000	15,750	30,870
EDG	**21**	**216**	**1,001**	**3,156**	**7,881**

Table 2. Values of the coefficient α_{NNZ} as a function of the number of spatial dimensions, the approximating polynomial order and the numerical discretization algorithm. This coefficient can be used in expression (10) to determine the total number of degrees of freedom in the problem.

III. The Navier-Stokes Equations

A. Governing Equations

We consider the steady-state compressible Navier-Stokes equations written in conservation form as

$$
\begin{aligned}
\boldsymbol{q} - \nabla \boldsymbol{u} &= 0, & \text{in } \Omega, \\
\nabla \cdot (\boldsymbol{F}(\boldsymbol{u}) + \boldsymbol{G}(\boldsymbol{u}, \boldsymbol{q})) &= 0, & \text{in } \Omega,
\end{aligned}
\tag{11}
$$

where $\boldsymbol{G}(\boldsymbol{u}, \boldsymbol{q})$ are the viscous fluxes of dimension $m \times d$. The nondimensional form of the Navier-Stokes equations as well as the definition of the inviscid and viscous fluxes can be found in [2]. The Navier-Stokes equations (11) should be supplemented with appropriate boundary conditions at the inflow, outflow and solid wall boundaries, and source term.

In addition to the notation introduced in Section II, we need to define a new approximation space as

$$
\boldsymbol{V}_h^k = \{\boldsymbol{v} \in (L^2(\mathcal{T}_h))^{m \times m} \; : \; \boldsymbol{v}|_K \in (\mathcal{P}^k(K))^{m \times m}, \; \forall \, K \in \mathcal{T}_h\}.
$$

The approximate gradient $\boldsymbol{q}_h$, which approximates $\boldsymbol{q}$, resides in this space.

B. The HDG Method for the Navier-Stokes Equations

Following the method of line for the Euler equations we seek an approximation $(\boldsymbol{q}_h, \boldsymbol{u}_h, \widehat{\boldsymbol{u}}_h) \in \boldsymbol{V}_h^k \times \boldsymbol{W}_h^k \times \boldsymbol{M}_h^k$ such that

$$
\begin{aligned}
(\boldsymbol{q}_h, \boldsymbol{v})_{\mathcal{T}_h} + (\boldsymbol{u}_h, \nabla \cdot \boldsymbol{v})_{\mathcal{T}_h} - \langle \widehat{\boldsymbol{u}}_h, \boldsymbol{v} \cdot \boldsymbol{n} \rangle_{\partial \mathcal{T}_h} &= 0, & \forall \boldsymbol{v} \in \boldsymbol{V}_h^k, \\
-(\boldsymbol{F}(\boldsymbol{u}_h) + \boldsymbol{G}(\boldsymbol{u}_h, \boldsymbol{q}_h), \nabla \boldsymbol{w})_{\mathcal{T}_h} + \left\langle (\widehat{\boldsymbol{F}}_h + \widehat{\boldsymbol{G}}_h) \cdot \boldsymbol{n}, \boldsymbol{w} \right\rangle_{\partial \mathcal{T}_h} &= 0, & \forall \boldsymbol{w} \in \boldsymbol{W}_h^k, \\
\left\langle (\widehat{\boldsymbol{F}}_h + \widehat{\boldsymbol{G}}_h) \cdot \boldsymbol{n}, \boldsymbol{\mu} \right\rangle_{\partial \mathcal{T}_h \backslash \partial \Omega} + \left\langle \widehat{\boldsymbol{B}}_h, \boldsymbol{\mu} \right\rangle_{\partial \Omega} &= 0, & \forall \boldsymbol{\mu} \in \boldsymbol{M}_h^k.
\end{aligned}
\tag{12}
$$

Here, the numerical fluxes $\widehat{\boldsymbol{F}}_h$ and $\widehat{\boldsymbol{G}}_h$ are an approximation to $\boldsymbol{F}(\boldsymbol{u})$ and $\boldsymbol{G}(\boldsymbol{u}, \boldsymbol{q})$ over ∂K, respectively. In addition, $\widehat{\boldsymbol{B}}_h$ is the numerical flux vector of dimension m defined over the boundary.

As before, we take the interior numerical fluxes of form

$$
(\widehat{\boldsymbol{F}}_h + \widehat{\boldsymbol{G}}_h) \cdot \boldsymbol{n} = (\boldsymbol{F}(\widehat{\boldsymbol{u}}_h) + \boldsymbol{G}(\widehat{\boldsymbol{u}}_h, \boldsymbol{q}_h)) \cdot \boldsymbol{n} + \boldsymbol{S}(\boldsymbol{u}_h, \widehat{\boldsymbol{u}}_h)(\boldsymbol{u}_h - \widehat{\boldsymbol{u}}_h),
\tag{13}
$$

where the stabilization matrix $\boldsymbol{S}$ can be selected by extending the form for the Euler equations as

$$
\boldsymbol{S} = (|\widehat{\boldsymbol{u}}_h \cdot \boldsymbol{n}| + c_h + \frac{\gamma}{PrRe})\boldsymbol{I}.
\tag{14}
$$

The definition of the boundary numerical flux $\widehat{\boldsymbol{B}}_h$ depends on the types of boundary conditions and can be found in [21].

C. The EDG Method for the Navier-Stokes Equations

The EDG method for the Navier-Stokes equations finds an approximation $(\boldsymbol{q}_h, \boldsymbol{u}_h, \widehat{\boldsymbol{u}}_h) \in \boldsymbol{V}_h^k \times \boldsymbol{W}_h^k \times \widetilde{\boldsymbol{M}_h}^k$ such that

$$
\begin{aligned}
(\boldsymbol{q}_h, \boldsymbol{v})_{\mathcal{T}_h} + (\boldsymbol{u}_h, \nabla \cdot \boldsymbol{v})_{\mathcal{T}_h} - \langle \widehat{\boldsymbol{u}}_h, \boldsymbol{v} \cdot \boldsymbol{n} \rangle_{\partial \mathcal{T}_h} &= 0, & \forall \boldsymbol{v} \in \boldsymbol{V}_h^k, \\
-(\boldsymbol{F}(\boldsymbol{u}_h) + \boldsymbol{G}(\boldsymbol{u}_h, \boldsymbol{q}_h), \nabla \boldsymbol{w})_{\mathcal{T}_h} + \left\langle (\widehat{\boldsymbol{F}}_h + \widehat{\boldsymbol{G}}_h) \cdot \boldsymbol{n}, \boldsymbol{w} \right\rangle_{\partial \mathcal{T}_h} &= 0, & \forall \boldsymbol{w} \in \boldsymbol{W}_h^k, \\
\left\langle (\widehat{\boldsymbol{F}}_h + \widehat{\boldsymbol{G}}_h) \cdot \boldsymbol{n}, \boldsymbol{\mu} \right\rangle_{\partial \mathcal{T}_h \backslash \partial \Omega} + \left\langle \widehat{\boldsymbol{B}}_h, \boldsymbol{\mu} \right\rangle_{\partial \Omega} &= 0, & \forall \boldsymbol{\mu} \in \widetilde{\boldsymbol{M}}_h^k.
\end{aligned}
\tag{15}
$$

Thus, the EDG method is very similar to the HDG method. The only difference between the two methods is the approximation space for the hybrid variable $\widehat{\boldsymbol{u}}_h$. This difference leads to differences in the number of degrees of freedom and the number of nonzero entries, as well as the sparsity pattern of their global matrix systems, as pointed out in Section II.

By applying the Newton-Raphson procedure to solve the nonlinear system (15) we obtain at every Newton step a matrix system of the form

$$
\begin{bmatrix}
A & B & E \\
C & D & L \\
M & N & P
\end{bmatrix}
\begin{pmatrix}
Q \\
U \\
\Lambda
\end{pmatrix}
=
\begin{pmatrix}
H \\
F \\
G
\end{pmatrix},
$$

where Q, U and Λ are the vectors of degrees of freedom of $\boldsymbol{q}_h$, $\boldsymbol{u}_h$ and $\widehat{\boldsymbol{u}}_h$, respectively. We note that the degrees of freedom for $\boldsymbol{q}_h$, $\boldsymbol{u}_h$ are grouped together and ordered in an element-wise fashion, the corresponding matrix $[A\ B; C\ D]$ has block-diagonal structure. The size of each block is given by the number of degrees of freedom of $\boldsymbol{q}_h$, $\boldsymbol{u}_h$ associated to each element. Therefore, we can eliminate both $\boldsymbol{Q}$ and U to obtain a reduced system in terms of Λ as

$$
\mathbb{A} \Lambda = \mathbb{F},
$$

where

$$
\mathbb{A} = P - \begin{bmatrix} M & N \end{bmatrix} \begin{bmatrix} A & B \\ C & D \end{bmatrix}^{-1} \begin{bmatrix} E \\ L \end{bmatrix}, \qquad \mathbb{F} = G - \begin{bmatrix} M & N \end{bmatrix} \begin{bmatrix} A & B \\ C & D \end{bmatrix}^{-1} \begin{bmatrix} H \\ F \end{bmatrix}.
$$

The matrix $\mathbb{A}$ has the same size and structure as the matrix $\mathbb{K}$ of the EDG method for the Euler equations.

D. Extension to the Unsteady Navier-Stokes Equations

Finally, we extend the EDG method to the unsteady Navier-Stokes equations

$$
\begin{aligned}
\boldsymbol{q} - \nabla \boldsymbol{u} &= 0, & \text{in } \Omega \times (0, t_f], \\
\frac{\partial \boldsymbol{u}}{\partial t} + \nabla \cdot (\boldsymbol{F}(\boldsymbol{u}) + \boldsymbol{G}(\boldsymbol{u}, \boldsymbol{q})) &= 0, & \text{in } \Omega \times (0, t_f], \\
\boldsymbol{u} &= \boldsymbol{u}_0, & \text{on } \Omega \times \{t = 0\}.
\end{aligned}
$$

The boundary conditions are the same as the steady-state case.

For simplicity of exposition we consider the Backward-Euler scheme to discretize the time derivative since time integration using high-order backward difference formulae (BDF) schemes and diagonally implicit Runge-Kutta (DIRK) methods admits a similar procedure. At time level $t^j = j\Delta t$ we seek an approximation $(\boldsymbol{q}_h^j, \boldsymbol{u}_h^j, \widehat{\boldsymbol{u}}_h^j) \in \boldsymbol{V}_h^k \times \boldsymbol{W}_h^k \times \widetilde{\boldsymbol{M}}_h^k$ such that

$$
\begin{aligned}
\left(\boldsymbol{q}_h^j, \boldsymbol{v} \right)_{\mathcal{T}_h} + (\boldsymbol{u}_h^j, \nabla \cdot \boldsymbol{v})_{\mathcal{T}_h} - \left\langle \widehat{\boldsymbol{u}}_h^j, \boldsymbol{v} \cdot \boldsymbol{n} \right\rangle_{\partial \mathcal{T}_h} &= 0, & \forall \boldsymbol{w} \in \boldsymbol{V}_h^k, \\
\left(\frac{\boldsymbol{u}_h^j}{\Delta t}, \boldsymbol{w} \right) - \left(\boldsymbol{F}(\boldsymbol{u}_h^j) + \boldsymbol{G}(\boldsymbol{u}_h^j, \boldsymbol{q}_h^j), \nabla \boldsymbol{w} \right)_{\mathcal{T}_h} + \left\langle (\widehat{\boldsymbol{F}}_h^j + \widehat{\boldsymbol{G}}_h^j) \cdot \boldsymbol{n}, \boldsymbol{w} \right\rangle_{\partial \mathcal{T}_h} &= \left(\frac{\boldsymbol{u}_h^{j-1}}{\Delta t}, \boldsymbol{w} \right), & \forall \boldsymbol{w} \in \boldsymbol{W}_h^k, \\
\left\langle (\widehat{\boldsymbol{F}}_h^j + \widehat{\boldsymbol{G}}_h^j) \cdot \boldsymbol{n}, \boldsymbol{\mu} \right\rangle_{\partial \mathcal{T}_h \backslash \partial \Omega} + \left\langle \widehat{\boldsymbol{B}}_h^j, \boldsymbol{\mu} \right\rangle_{\partial \Omega} &= 0, & \forall \boldsymbol{\mu} \in \widetilde{\boldsymbol{M}}_h^k.
\end{aligned}
\tag{16}
$$

As before, we define the interior numerical fluxes as

$$(\widehat{\boldsymbol{F}}_h^j + \widehat{\boldsymbol{G}}_h^j) \cdot \boldsymbol{n} = (\boldsymbol{F}(\widehat{\boldsymbol{u}}_h^j) + \boldsymbol{G}(\widehat{\boldsymbol{u}}_h^j, \boldsymbol{q}_h^j)) \cdot \boldsymbol{n} + \boldsymbol{S}(\boldsymbol{u}_h^j, \widehat{\boldsymbol{u}}_h^j)(\boldsymbol{u}_h^j - \widehat{\boldsymbol{u}}_h^j), \tag{17}$$

and the boundary numerical flux $\widehat{\boldsymbol{B}}_h^j$ as already described in the previous subsection. Since this discrete nonlinear system is similar to the system (15) for the steady-state case, we apply the same solution procedure described above for the steady-state case to the time-dependent case at every time level.

IV.   Numerical Results

A.   Ringleb flow

We first consider the Ringleb flow to demonstrate the optimal accuracy of both the EDG and HDG methods. The Ringleb flow is an exact smooth solution of the Euler equations obtained using the hodograph method.[4] For any given (x, y), we first obtain the radial velocity V by solving the following nonlinear equation

$$(x - 0.5L^2) + y^2 = \frac{1}{4\rho^2 V^4},$$

where

$$c = \sqrt{1 - \frac{V^2}{5}}, \quad \rho = c^5, \quad L = \frac{1}{c} + \frac{1}{3c^3} + \frac{1}{5c^5} - \frac{1}{2}\ln\frac{1+c}{1-c}.$$

We then compute the exact solution as

$$\rho = c^5, \quad p = c^7/\gamma, \quad v_1 = V\cos(\theta), \quad v_2 = V\sin(\theta),$$

where

$$\psi = \sqrt{\frac{1}{2V^2} - (x - 0.5L)\rho}, \qquad \theta = \arcsin(\psi V).$$

Since the exact solution can be determined for any spatial point, we take the domain Ω to be $(-2, -1) \times (1, 2)$. The boundary condition is prescribed by setting the freestream value $\boldsymbol{u}_\infty$ to the exact solution on the boundary of the domain. We consider triangular meshes that are obtained by splitting a regular $n \times n$ Cartesian grid into $2n^2$ triangles. On these meshes, we use polynomials of degree k to represent all the approximate variables with a nodal basis.

We present the L^2 error and convergence rate of the numerical solution $\boldsymbol{u}_h$ as a function of h and k in Table 3 for the HDG method and in Table 4 for the EDG method. We observe that the approximate solution converges with the optimal order $k + 1$ for both the HDG and EDG methods.

| mesh | $k = 1$ | | $k = 2$ | | $k = 3$ | | $k = 4$ | |
$1/h$	error	order	error	order	error	order	error	order
2	4.35e-3	––	3.24e-4	––	2.35e-5	––	2.08e-6	––
4	1.10e-3	1.98	4.85e-5	2.74	1.43e-6	4.04	7.90e-8	4.72
8	2.80e-4	1.98	6.92e-6	2.81	8.63e-8	4.05	2.80e-9	4.82
16	7.06e-5	1.99	9.37e-7	2.88	5.18e-9	4.06	9.36e-11	4.90
32	1.77e-5	2.00	1.22e-7	2.94	3.83e-10	3.76	3.09e-12	4.92

Table 3. History of convergence of the HDG method for the Ringleb flow.

B.   Steady viscous flow past a Kármán-Trefftz airfoil

The second example we consider is steady viscous flow over a Kármán-Trefftz airfoil. The flow conditions are $M_\infty = 0.1$, $Re = 4,000$ and an angle of attach $\alpha = 0$. The geometry of the airfoil is obtained by conformal mapping using a Kármán-Trefftz transformation.[21] The airfoil geometry as well as a detail of the mesh

American Institute of Aeronautics and Astronautics

mesh	$k=1$		$k=2$		$k=3$		$k=4$	
$1/h$	error	order	error	order	error	order	error	order
2	4.31e-3	$--$	3.52e-4	$--$	2.47e-5	$--$	2.32e-6	$--$
4	1.08e-3	2.00	5.99e-5	2.56	1.50e-6	4.05	9.21e-8	4.65
8	2.76e-4	1.97	9.93e-6	2.59	8.74e-8	4.10	3.56e-9	4.69
16	7.00e-5	1.98	1.51e-6	2.72	5.14e-9	4.09	1.60e-10	4.48
32	1.75e-5	2.00	2.13e-7	2.83	3.62e-10	3.83	5.41e-12	4.89

Table 4. History of convergence of the EDG method for the Ringleb flow.

utilized is shown in Figure 1. The mesh employed for all computations has 1280 triangular elements. We use polynomials of degree k to represent both the numerical solution and curved elements.

We present in Figure 1 the Mach number contour of the solution computed using the EDG method with $k = 4$. In Figure 2, we compare the distributions of pressure coefficient and skin friction coefficient over the airfoil surface, computed using the EDG scheme and the HDG scheme. We observe that the two schemes yield very similar results. We note however that the number of globally coupled unknowns for the EDG scheme and HDG scheme is 26,112 and 39,040, respectively.

C. Unsteady viscous flow over a SD7003 airfoil

The third test case is the compressible viscous flow passing a SD7003 foil[24] at the Reynolds number $Re = 10,000$, $M_\infty = 0.1$, and $\alpha = 5^o$. The FE mesh has 1728 elements as shown in Figure 3. We use $k = 5$ for spatial discretization and the DIRK(3,3) scheme with a timestep size $\Delta t = 0.04$ for time integration. We observe the vortex shedding behind the airfoil as depicted in Figure 4. Figure 5 depicts the time history of drag and lift coefficients which show that the flow is nearly periodic. The average lift coefficient is 0.4750 and the average drag coefficient is 0.0605.

D. Inviscid transonic flow past a Kármán-Trefftz airfoil

We now consider inviscid transonic flow past a Kármán-Trefftz airfoil at a freestream mach number of $M_\infty = 0.8$ and an angle of attack of 5.0 degrees. A weak shock is formed on the upper surface near the trailing edge. In order to deal with shock waves, we employ the artificial viscosity approach proposed in [19]. In this example, we use a finite element mesh of only 400 triangles. Isoparametric elements with the polynomials of degree $k = 4$ are used to represent both the solution and geometry. We present the numerical results in Figure 6 for both the HDG scheme and the EDG scheme. We observe that our schemes captures shock very well at the sub-cell level.

E. Inviscid supersonic flow past a circular duct

This test case involves inviscid supersonic flow in a channel with a 4% thick circular bump on the bottom side. The length and height of the channel are 3 and 1, respectively. The inlet Mach number is $M_\infty = 1.4$. Inlet/outlet conditions are prescribed at the left/right boundaries, while inviscid wall boundary condition is used on the top and bottom sides. The physical domain is discretized into 600 triangular elements. Isoparametric elements with the polynomials of degree $k = 4$ are used to represent both the unknowns and geometry. We present in Figure 7 the density, Mach number, and artificial viscosity obtained by using the HDG scheme and the EDG scheme. We observe that the shocks are sharp and smooth and that artificial viscosity is added only to the shock region.

F. Turbulent flow past a flat plate

We consider the incompressible flow over a smooth flat plate studied experimentally by Wieghardt and included in the 1968 AFOSR-IFP Stanford Conference as a validation case of CFD codes.[5] The Reynolds number is 2.1854×10^{-6}. The freestream Mach number is set to 0.2 to accelerate the convergence of the

American Institute of Aeronautics and Astronautics

compressible flow codes. We use a finite element mesh of 572 triangular elements as shown in 8. Grid lines are clustered around the leading edge of the plate to resolve flow gradients there and around the wall surface to resolve the boundary layer. The first grid point off the wall is at a distance of 1.29×10^{-4} from the wall surface. Of course, our DG meshes constructed upon this grid have the resolution scaled up with the polynomial order.

Here we solve Reynolds-averaged Navier-Stokes (RANS) equations which include the Navier-Stokes equations and turbulence model equations. The Spalart-Allmaras (SA) equation[23] is used here to model turbulent flows. It is known that the SA equation is very stiff and difficult to integrate with using high-order methods.[20] Therefore, we employ a modified version of the original SA turbulence model proposed in [11]. It is shown in [11] that the modified SA model works well for many cases where the original SA model fails. Indeed, the original SA model did not converge for this particular test case.

We start with a uniform flow field at freestream conditions and integrate in time using the implicit backward Euler method with adaptive step size control to find the steady-state solution. The EDG scheme is used to compute the solution. We first present in Figure 9 the eddy viscosity for $k = 2$ and $k = 4$. We observe that the eddy viscosity are quite smooth although the grid used is pretty coarse.

We next present the computed turbulent quantities and make comparison with the experimental data obtained by Wieghardt[5] and with the law of the wall theory. The near wall behavior of the flow field in terms of the non-dimensional velocity profile $u^+ = u/u_\tau$ versus $y^+ = yu_\tau/\nu$ at $Re_x = 1.02 \times 10^7$ is shown in Figure 10(a) for several polynomial orders; here $u_\tau = \sqrt{\nu \partial u/\partial y(y = 0)}$ is the friction velocity. We see that the computed velocity profiles match excellently with the experimental data in the log layer and with the law of the for velocity in the viscous sublayer. Note that the law of the wall for velocity profile takes after Spalding's formula[25] which has been confirmed by experiment as an excellent fit to inner-law data in the viscous sublayer. Figure 10(b) shows the skin friction distribution over the plate for the same polynomial orders and for the experimental measurements. We observe that the $k = 2$ solution yields oscillatory skin friction distribution near the leading edge, while the $k = 4$ solution gives much smoother distribution. Overall, the skin friction predictions are in good agreement with the experimental data. We would like to point out that good results are obtained even for a pretty coarse grid.

G. Turbulent subsonic flow past a NACA 0012 foil

We finally present results for the fully turbulent flow past NACA 0012 airfoil at Mach number $M_\infty = 0.3$, Reynolds number of 1.85×10^6, and zero angle-of-attack. We use a single-block, two-dimensional C-grid of 2304 triangular elements as shown in Figure 11. The grid is clustered around the leading edge and the trailing edge to resolve the flow gradients there, and around the airfoil surface to resolve the boundary layer on the airfoil. The first grid point off the wall is at a distance of 2.02×10^{-5} from the airfoil surface. Our DG meshes constructed upon this grid have the resolution scaled up with the polynomial order. The EDG scheme is used to compute the numerical results.

We present the eddy viscosity contour in Figure 12 and Mach number contour in Figure 13. We present in Figure 14 the pressure coefficient distribution for polynomial orders of $p = 2$, $p = 3$ and $p = 4$. We see that numerical predictions agree quite well with the experimental measurements reported in [1].

V.   Conclusions

We have presented an Embedded Discontinuous Galerkin method for the numerical solution of the compressible Euler and Navier-Stokes equations. The proposed method holds important advantages over many existing DG methods in terms of the globally coupled degrees of freedom. The accuracy of the solution obtained with the EDG method appears to be comparable to that obtained with the HDG method for many test cases.

References

[1] AGARD, *Experimental Data Base for Computer Program Assessment*, Report of the Fluid Dynamics Panel Working Group 04, AGARD-AR-138, May 1979.

[2] D. A. Anderson, J. C. Tannehill, and R. H. Pletcher, *Computational Fluid Dynamics and Heat Transfer*. Hemisphere Publishing, New York, 1984.

American Institute of Aeronautics and Astronautics

[3] F. Bassi and S. Rebay, A high-order accurate discontinuous finite element method for the numerical solution of the compressible Navier-Stokes equations. *J. Comput. Phys.*, 131:267–279, 1997.

[4] G. Chiocchia, Exact solutions to transonic and supersonic flows. Technical Report AR-211, AGARD, 1985.

[5] D. E. Coles and E. A. Hirst, *Computation of Turbulent Boundary Layers*, AFOSR-IFP-Stanford Conference, Vol. II, Stanford University, CA, 1969.

[6] B. Cockburn, J. Gopalakrishnan, and R. Lazarov, Unified hybridization of discontinuous Galerkin, mixed and continuous Galerkin methods for second order elliptic problems. *SIAM J. Numer. Anal.*, 47:1319–1365, 2009.

[7] B. Cockburn, B. Dong, J. Guzman, M. Restelli, and R. Sacco, A Hybridizable Discontinuous Galerkin Method for Steady-State Convection-Diffusion-Reaction Problems *SIAM J. Sci. Comput.* 31:3827, 2009.

[8] B. Cockburn, J. Gopalakrishnan, N. C. Nguyen, J. Peraire, and F-J Sayas, Analysis of an HDG method for Stokes flow. *Math. Comp.*. 80:723–760, 2011.

[9] B. Cockburn, J. Guzman, S.C. Soon, H. K. Stolarski, An Analysis of the Embedded Discontinuous Galerkin Method for Second-Order Elliptic Problems *SIAM J. Numer. Anal.*, 47(4):2686-2707, 2009.

[10] S. Güzey, B. Cockburn, and H.K. Stolarski, The embedded discontinuous Galerkin methods: Application to linear shells problems, Int.. J. Numer. Methods Engrg. 70 (2007), 757 790.

[11] D. Moro, N.C. Nguyen and J. Peraire, Navier-Stokes solution using hybridizable discontinuous Galerkin methods. presented at AIAA Conference, Hononulu, HI, June 2011.

[12] N. C. Nguyen, J. Peraire, and B. Cockburn, An implicit high-order hybridizable discontinuous Galerkin method for linear convection-diffusion equations. *J. Comput. Phys.*, 228:3232–3254, 2009.

[13] N. C. Nguyen, J. Peraire, and B. Cockburn, An implicit high-order hybridizable discontinuous Galerkin method for nonlinear convection-diffusion equations. *J. Comput. Phys.*, 228:8841–8855, 2009.

[14] N.C. Nguyen, J. Peraire, and B. Cockburn, A hybridizable discontinuous Galerkin method for Stokes flow. *Computer Methods in Applied Mechanics and Engineering,* 199:582-597, 2010

[15] N.C. Nguyen, J. Peraire, and B. Cockburn, A comparison of HDG methods for Stokes flow. Journal of Scientific Computing, 45(1-3):215-237, 2010.

[16] N.C. Nguyen, J. Peraire, and B. Cockburn, A hybridizable discontinuous Galerkin method for the incompressible Navier-Stokes equations. *J. Comput. Phys.*, 230:1147–1170, 2011.

[17] N. C. Nguyen, J. Peraire, and B. Cockburn. A hybridizable discontinuous Galerkin method for the incompressible Navier-Stokes equations (AIAA Paper 2010-362). In *Proceedings of the 48th AIAA Aerospace Sciences Meeting and Exhibit*, Orlando, Florida, Janury 2010.

[18] N. C. Nguyen, J. Peraire, and B. Cockburn. Hybridizable discontinuous Galerkin methods, *in Spectral and High Order Methods for Partial Differential Equations*, (Editors J. S. Hesthaven and E. M. Ronquist). *Lecture Notes in Computational Science and Engineering*, 2011, Volume 76, pages 63-84.

[19] N.C. Nguyen and J. Peraire, An adaptive shock-capturing HDG method for compressible flows presented at AIAA Conference, Hononulu, HI, June 2011.

[20] N. C. Nguyen, P. O. Persson, and J. Peraire, RANS Solutions using high order discontinuous Galerkin methods. In Proceedings of the 45th AIAA Aerospace Sciences Meeting and Exhibit, AIAA-2007-0914, Reno, NV, January 2007.

[21] J. Peraire, N.C. Nguyen and B. Cockburn, A hybridizable discontinuous Galerkin method for the compressible Euler and Navier-Stokes equations', presented at AIAA Conference, AIAA-2010-363, Orlando, FL, January 2010

[22] J. Peraire and P. O. Persson, The compact discontinuous Galerkin (CDG) method for elliptic problems. *SIAM Journal on Scientific Computing*, 30(4):1806–1824, 2008.

[23] P. R. Spalart and S. R. Allmaras, A one-equation turbulence model for aerodynamic flows, *La Rech. Aérospatiale* 1: 5–21, 1994.

[24] A. Uranga, P. O. Persson, M. Drela, and J. Peraire. Implicit large eddy simulation of transitional flows over airfoils and wings (AIAA Paper 2009-4131). In *Proceedings of the AIAA Computational Fluid Dynamics Conference*, San Antonio, TX, June 2009.

[25] F. M. White, *Viscous Fluid Flow*, 2nd Edition, McGraw-Hill, New York, 1991.
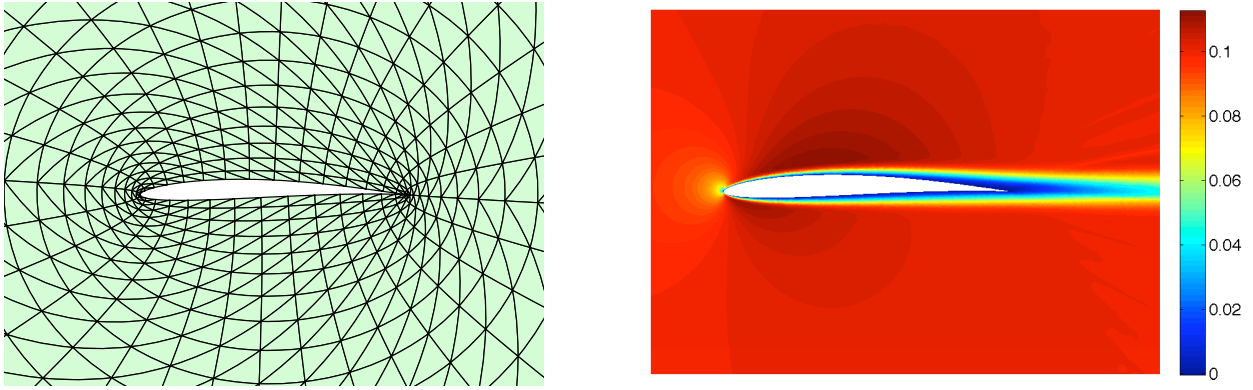
Figure 1. Viscous flow over a Kármán-Trefftz airfoil: $M_\infty = 0.1$, $Re = 4,000$, and $\alpha = 0$. Detail of the mesh employed (left) and Mach number contours of the solution (right) computed using the EDG method with $k = 4$.
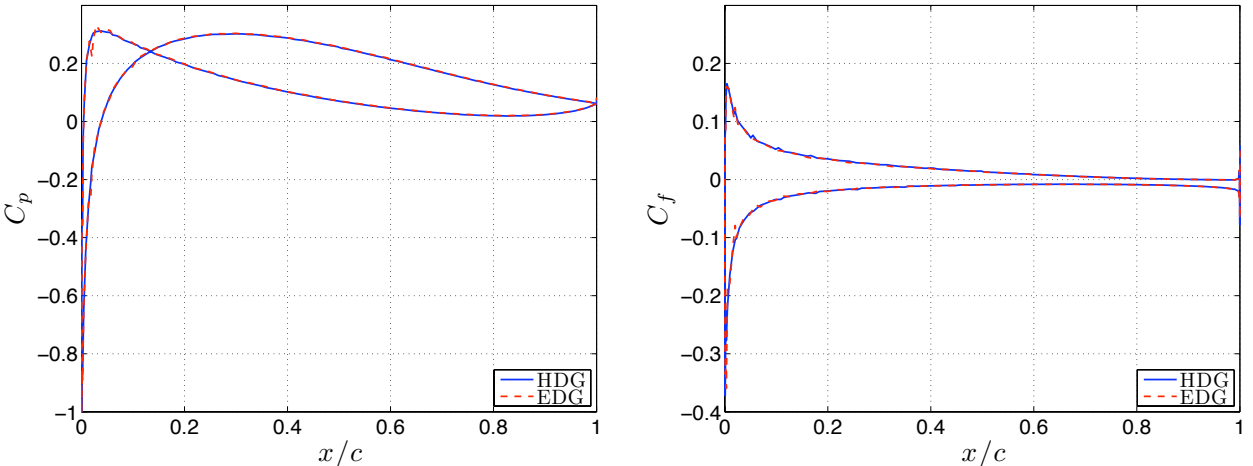

Figure 2. Viscous flow over a Kármán-Trefftz airfoil: $M_\infty = 0.1$, $Re = 4,000$, and $\alpha = 0$. The pressure coefficient (left) and skin friction coefficient (right) computed using $k = 4$ for the HDG and EDG algorithms.
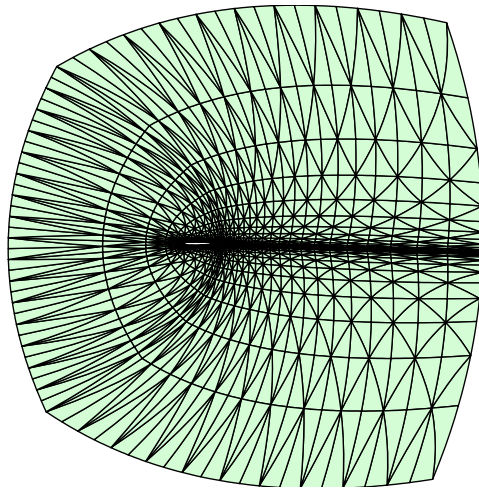
American Institute of Aeronautics and Astronautics

Figure 3. Finite element mesh for the SD7003 foil.
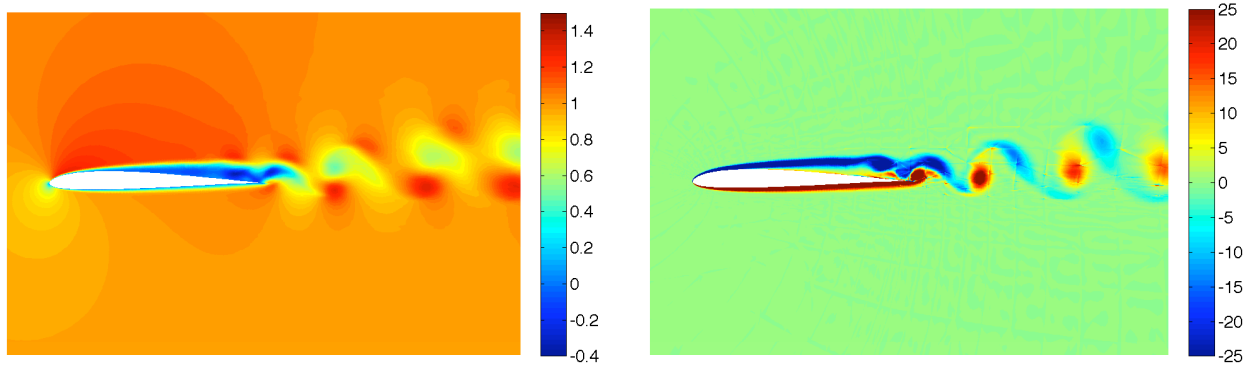
Figure 4. Horizontal velocity and vorticity at $t = 19.84$ **for compressible viscous flow past a SD7003 foil at** $Re = 10^4$, $M_\infty = 0.1$, **and** $\alpha = 5^o$.
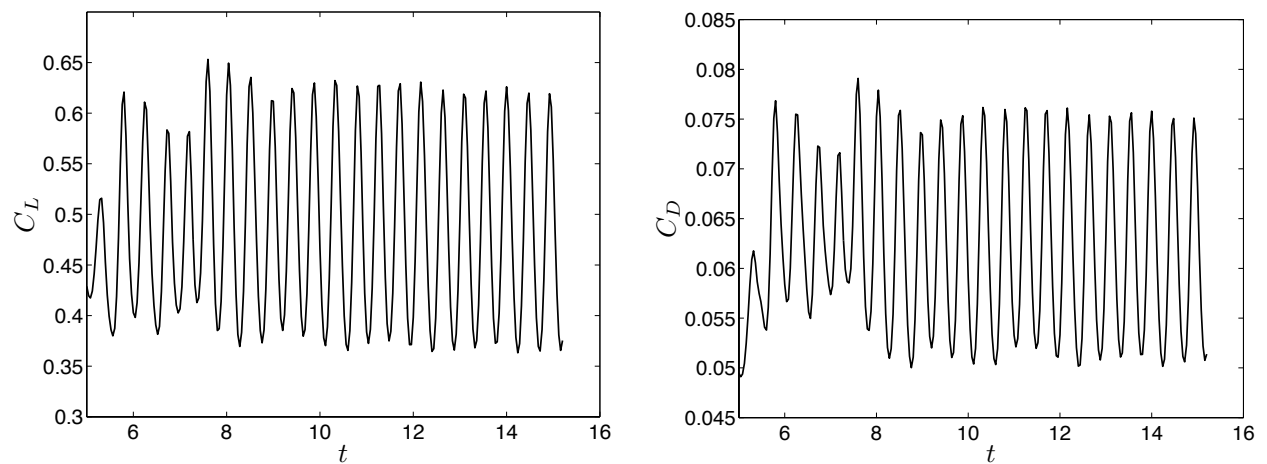
Figure 5. Time history of lift and drag coefficients for compressible viscous flow past a SD7003 foil at $Re = 10^4$, $M_\infty = 0.1$, **and** $\alpha = 5^o$.
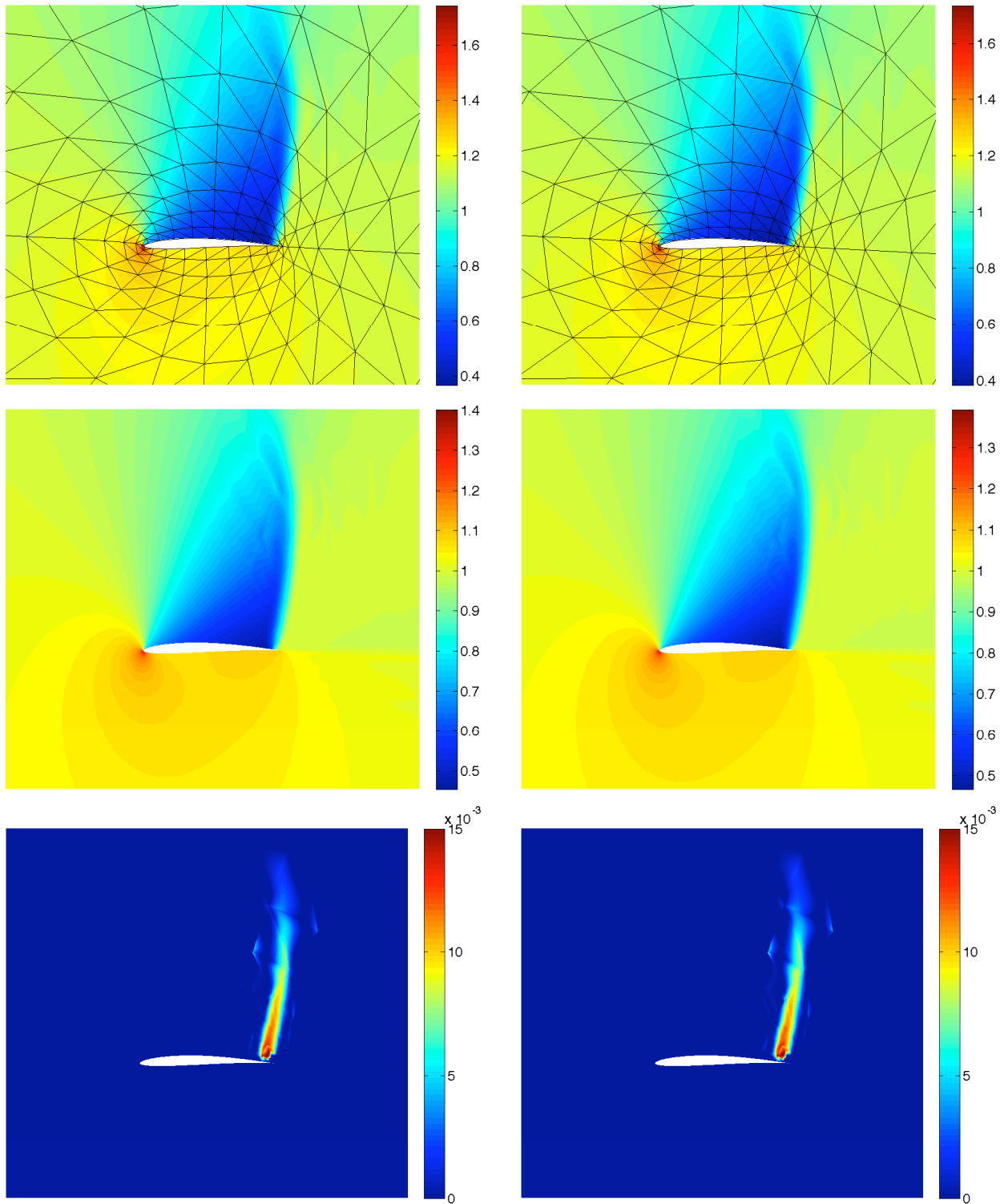
Figure 6. Inviscid transonic flow over a Kármán-Trefftz airfoil at $M_\infty = 0.8$ and $\alpha = 5^o$. Figures show the pressure (top), density (middle), and artificial viscosity (bottom) for the HDG method (left) and the EDG method (right).

American Institute of Aeronautics and Astronautics
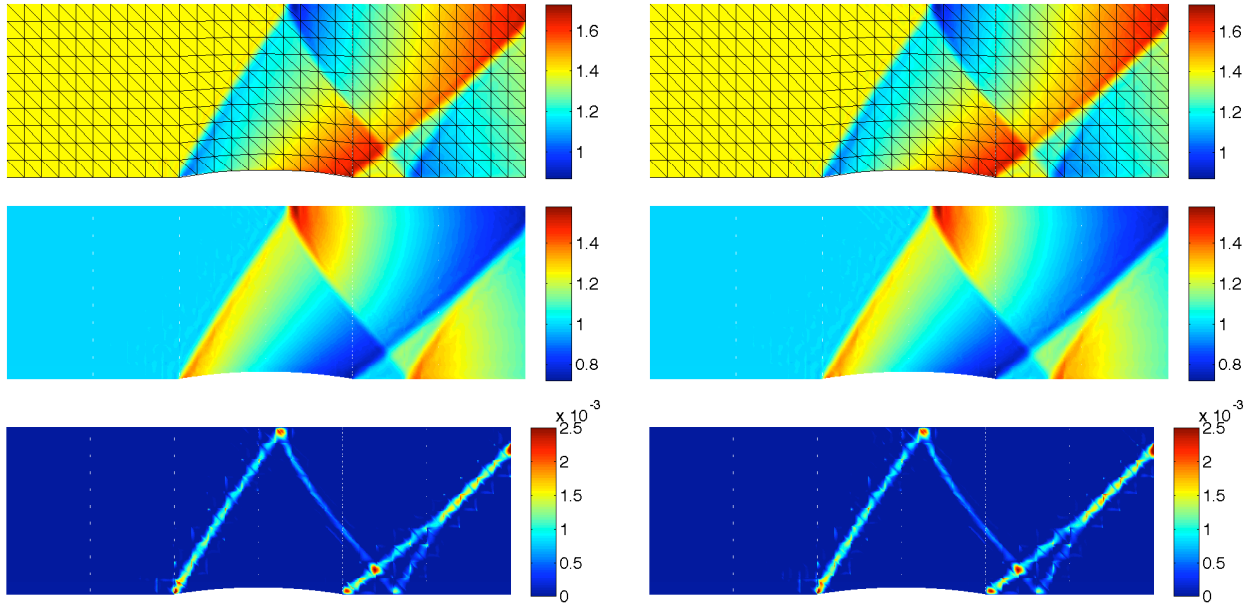
Figure 7. Inviscid supersonic flow past a circular duct at $M_\infty = 1.4$. Figures show the Mach number (top), density (middle), and artificial viscosity (bottom) for the HDG method (left) and the EDG method (right).
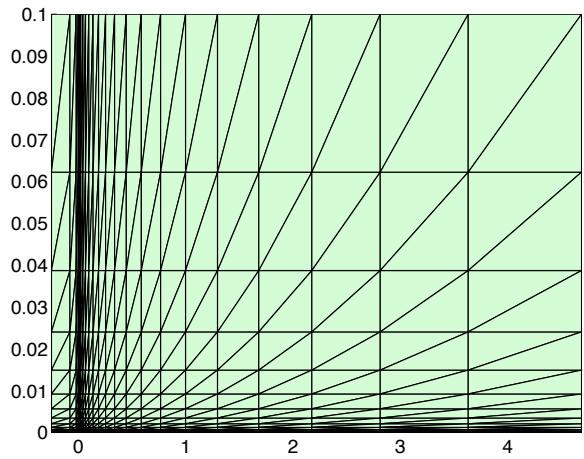
Figure 8. Finite element mesh for the flat plate.
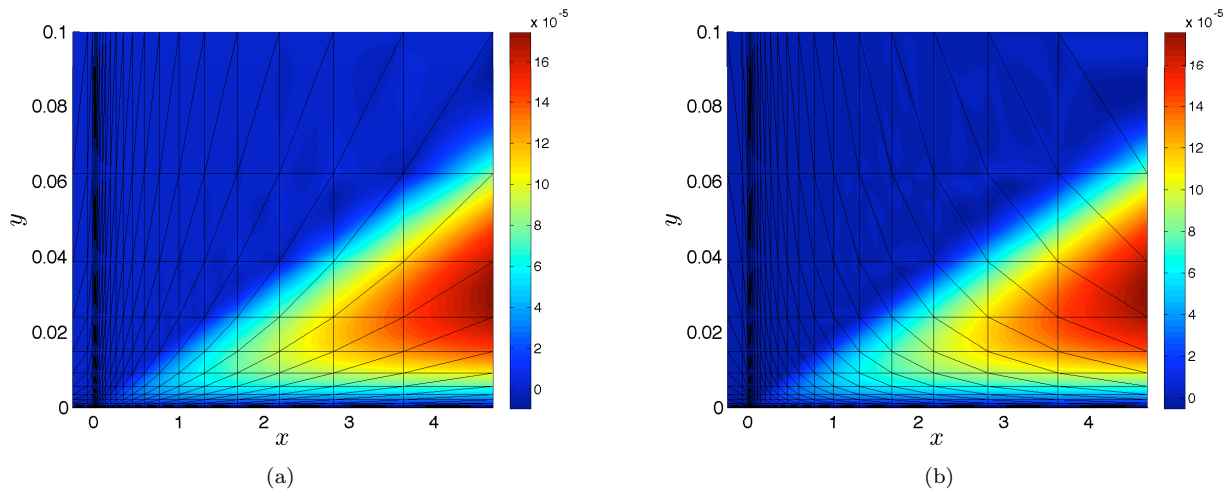
Figure 9. Eddy viscosity contours of the solution computed using the EDG scheme for $k = 2$ (left) and $k = 4$ (right). Note that the axes are of different scales.
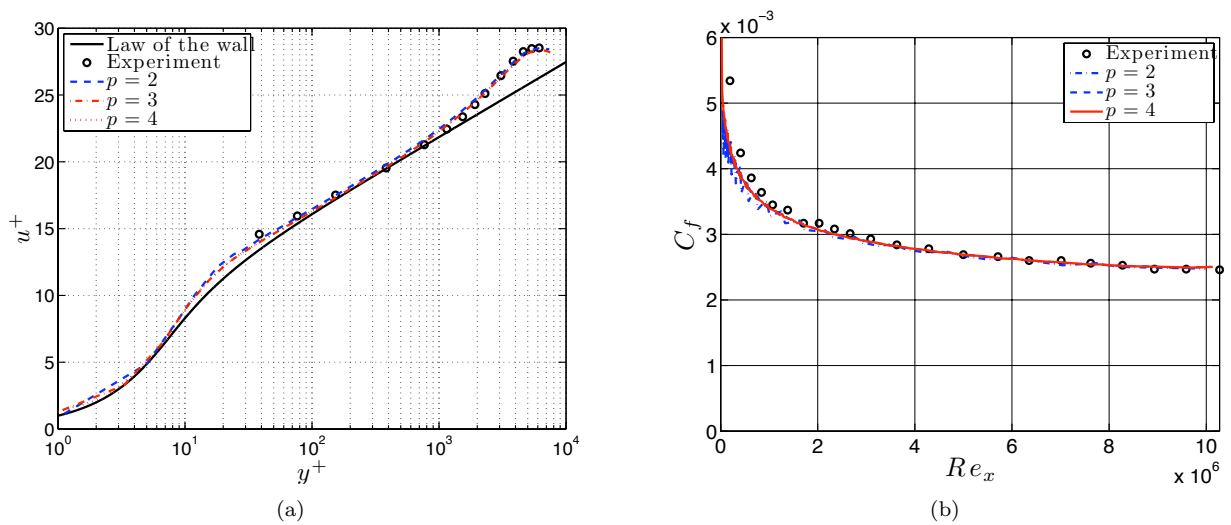

Figure 10. Comparison between the computed turbulent quantities and the experimental data in a flat-plate boundary layer: (a) velocity profiles at $Re_x = 1.02 \times 10^7$ and (b) skin friction coefficient as function of Re_x.
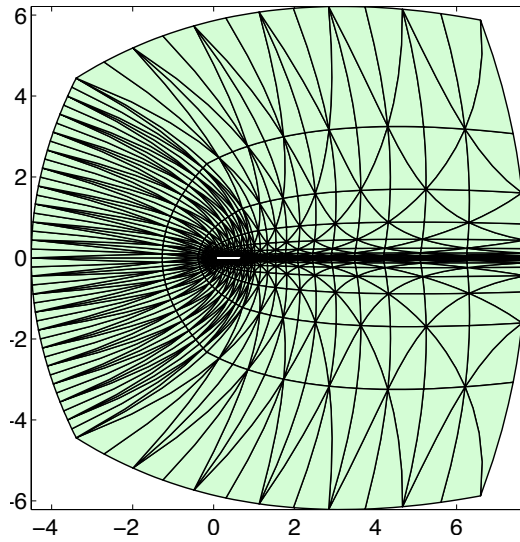
American Institute of Aeronautics and Astronautics

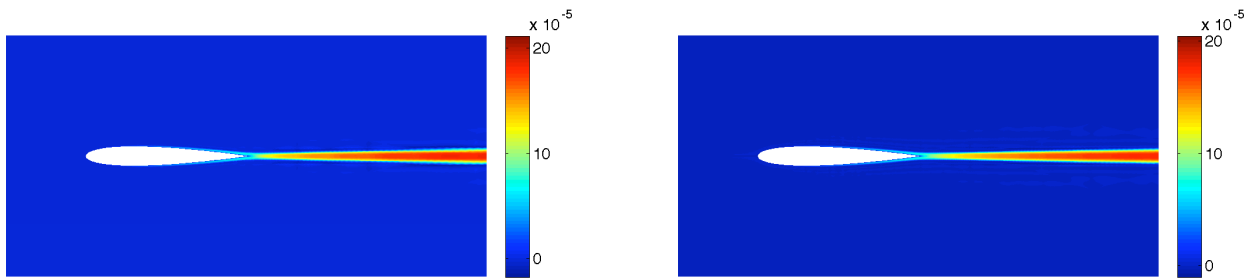**Figure 11. Finite element mesh for the NACA 0012 airfoil.**

Figure 12. Eddy viscosity contours of the solution computed using the EDG scheme for $k = 2$ (left) and $k = 4$ (right).
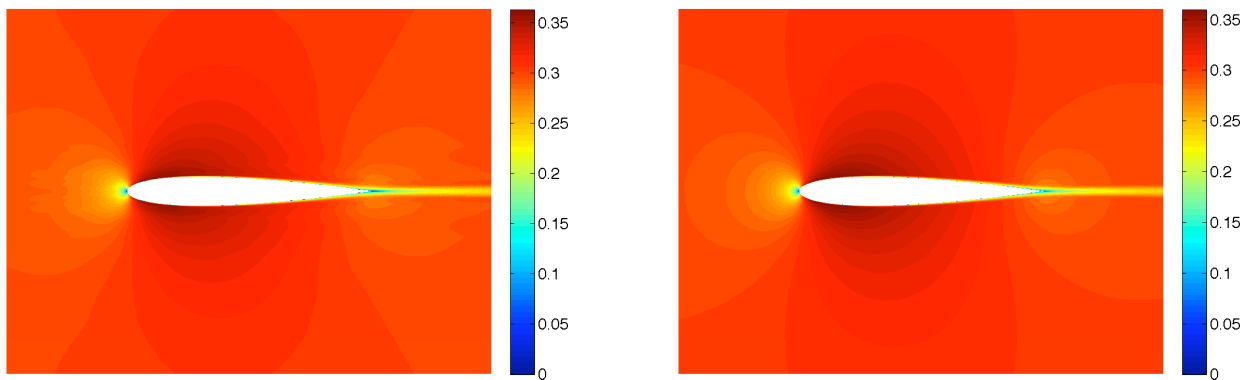

Figure 13. Mach number contours of the solution computed using the EDG scheme for $k = 2$ (left) and $k = 4$ (right). Note that the axes are of different scales.
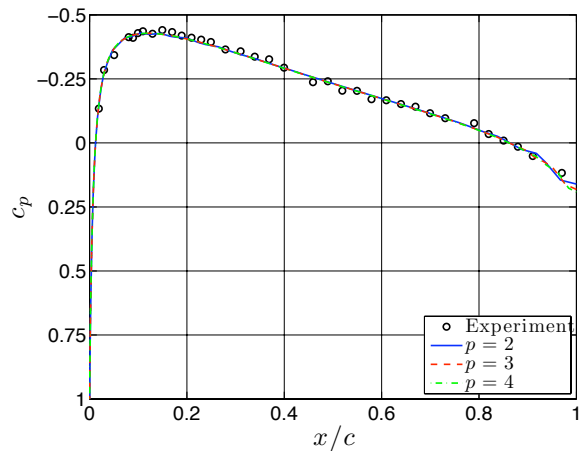
American Institute of Aeronautics and Astronautics

Figure 14. Pressure coefficient distribution over the airfoil surface.

American Institute of Aeronautics and Astronautics